

Influence of exchange bias on spin torque ferromagnetic resonancefor quantification of spin-orbit torque efficiency

Qian Zhao(赵乾), Tengfei Zhang(张腾飞), Bin He(何斌), Zimu Li(李子木), Senfu Zhang(张森富), GuoqiangYu(于国强), Jianbo Wang(王建波), Qingfang Liu(刘青芳), and Jinwu Wei(魏晋武)

Citation: Chin. Phys. B, 2024, 33 (**5**): 058502. DOI: 10.1088/1674-1056/ad2d55
Journal homepage: http://cpb.iphy.ac.cn; http://iopscience.iop.org/cpb

What follows is a list of articles you may be interested in

Interfacial DMI in Fe/Pt thin films grown on different buffer layers

Wen-Jun Zhang(张文君), Fei Wei(魏菲), Bing Liu(刘冰), Yang Zhou(周阳), Shi-Shou Kang(康仕寿), and Bing Sun(孙兵)

Chin. Phys. B, 2024, 33 (**4**): 048501. DOI: 10.1088/1674-1056/ad1b41

Valleytronic topological filters in silicene-like inner-edge systems

Hang Xie(谢航), Xiao-Long Lü(吕小龙), and Jia-En Yang(杨加恩)

Chin. Phys. B, 2024, 33 (**1**): 018502. DOI: 10.1088/1674-1056/ad0714

Ta thickness effect on field-free switching and spin-orbit torque efficiency in a ferromagnetically coupled Co/Ta/CoFeB trilayer

Zhongshu Feng(冯重舒), Changqiu Yu(于长秋), Haixia Huang(黄海侠), Haodong Fan(樊浩东),Mingzhang Wei(卫鸣璋), Birui Wu(吴必瑞), Menghao Jin(金蒙豪), Yanshan Zhuang(庄燕山),Ziji Shao(邵子霁), Hai Li(李海), Jiahong Wen(温嘉红), Jian Zhang(张鉴), Xuefeng Zhang(张雪峰),Ningning Wang(王宁宁), Sai Mu(穆赛), and Tiejun Zhou(周铁军)

Chin. Phys. B, 2023, 32 (**4**): 048504. DOI: 10.1088/1674-1056/aca7e9

Room-temperature electric control of exchange bias effect in $CoO_{1-\delta}$/Co films using $Pb(Mg_{1/3}Nb_{2/3})_{0.7}Ti_{0.3}O_3$ (110) substrates

Xin Wen(闻馨), Rui Wu(吴锐), Wen-Yun Yang(杨文云), Chang-Sheng Wang(王常生), Shun-Quan Liu(刘顺荃), Jing-Zhi Han(韩景智), Jin-Bo Yang(杨金波)

Chin. Phys. B, 2020, 29 (**9**): 098503. DOI: 10.1088/1674-1056/aba611

Perpendicular magnetization switching by large spin—orbit torques from sputtered Bi_2Te_3

Zhenyi Zheng(郑臻益), Yue Zhang(张悦), Daoqian Zhu(朱道乾), Kun Zhang(张昆), Xueqiang Feng(冯学强), Yu He(何宇), Lei Chen(陈磊), Zhizhong Zhang(张志仲), Dijun Liu(刘迪军), Youguang Zhang(张有光), Pedram Khalili Amiri, Weisheng Zhao(赵巍胜)

Chin. Phys. B, 2020, 29 (**7**): 078505. DOI: 10.1088/1674-1056/ab9439

Influence of exchange bias on spin torque ferromagnetic resonance for quantification of spin–orbit torque efficiency

Qian Zhao(赵乾)[1], Tengfei Zhang(张腾飞)[1], Bin He(何斌)[2,3], Zimu Li(李子木)[1], Senfu Zhang(张森富)[1], Guoqiang Yu(于国强)[2,3], Jianbo Wang(王建波)[1,4], Qingfang Liu(刘青芳)[1], and Jinwu Wei(魏晋武)[1,†]

[1] *Key Laboratory for Magnetism and Magnetic Materials of the Ministry of Education, Lanzhou University, Lanzhou* 730000, *China*
[2] *Beijing National Laboratory for Condensed Matter Physics, Institute of Physics, Chinese Academy of Sciences, Beijing* 100190, *China*
[3] *Center of Materials Science and Optoelectronics Engineering, University of Chinese Academy of Sciences, Beijing* 100049, *China*
[4] *Key Laboratory of Special Functional Materials and Structural Design, Ministry of Education, Lanzhou University, Lanzhou* 730000, *China*

(Received 21 November 2023; revised manuscript received 22 February 2024; accepted manuscript online 27 February 2024)

Antiferromagnet (AFM)/ferromagnet (FM) heterostructure is a popular system for studying the spin–orbit torque (SOT) of AFMs. However, the interfacial exchange bias field induces that the magnetization in FM layer is noncollinear to the external magnetic field, namely the magnetic moment drag effect, which further influences the characteristic of SOT efficiency. In this work, we study the SOT efficiencies of IrMn/NiFe bilayers with strong interfacial exchange bias by using spin-torque ferromagnetic resonance (ST-FMR) method. A full analysis on the AFM/FM systems with exchange bias is performed, and the angular dependence of magnetization on external magnetic field is determined through the minimum rule of free energy. The ST-FMR results can be well fitted by this model. We obtained the relative accurate SOT efficiency $\xi_{\mathrm{DL}} = 0.058$ for the IrMn film. This work provides a useful method to analyze the angular dependence of ST-FMR results and facilitates the accurate measurement of SOT efficiency for the AFM/FM heterostructures with strong exchange bias.

Keywords: antiferromagnets, spin–orbit torque, exchange bias, spin torque ferromagnetic resonance

PACS: 85.75.–d, 75.50.Ee, 76.50.+g **DOI:** 10.1088/1674-1056/ad2d55

Antiferromagnets (AFMs) are a promising candidate to enable new applications of spintronics in memory, computing, and terahertz devices due to their numerous features: the robustness against external magnetic field, absence of stray field, and ultrafast dynamics.[1–5] Recently, metallic AFMs were used to produce a large charge-to-spin conversion efficiency for the purpose of switching magnetization based on spin–orbit torque (SOT). To date, many researches have reported the large SOT efficiency in metallic AFMs, which generally originate from the strong spin–orbit coupling effect.[6–11] In addition, many fascinating characteristics were also observed, for instance, anisotropic or anomalous SOT in the epitaxial grown IrMn,[12,13] generation of out-of-plane spin polarization in noncollinear AFMs,[14–18] field-free magnetization switching in AFM/FM structures due to the exchange bias.[19–22] To better employ the metallic AFMs in magnetization switching, it is crucial to quantitatively characterize the SOT efficiency. However, the interfacial exchange bias in an ferromagnet (FM)/AFM bilayer influences the analysis of SOT efficiency. This makes the measured SOT efficiencies of AFMs be very diverging. A popular method is to insert the Cu layer between AFM and FM to eliminate the exchange bias.[23–25] However, this introduces an additional interface and extends the transmission path of spin current, which thus influences the accurate measurement of SOT efficiency. Therefore, it is necessary to clarify exactly how the exchange bias affect the delivery of SOT efficiencies of metallic AFMs.

Spin torque ferromagnetic resonance (ST-FMR)[25–28] and second harmonic Hall voltage[29–31] have been utilized to measure the SOT efficiency. When performing these two methods on a heavy metal (HM)/FM bilayer with in-plane magnetized FM, it is essential to analysis the angular dependence of static magnetization $\boldsymbol{M}_0$ on external magnetic field $\boldsymbol{H}_{\mathrm{ext}}$. Because the $\boldsymbol{M}_0$ is parallel to the $\boldsymbol{H}_{\mathrm{ext}}$ on the condition that $\boldsymbol{H}_{\mathrm{ext}}$ is larger than saturation field, the azimuth angle of $\boldsymbol{M}_0$ is equal to that of $\boldsymbol{H}_{\mathrm{ext}}$, i.e., $\varphi_M = \varphi_H$. Consequently, one can easily obtain the SOT efficiency of HM, or untraditional spin polarization, by analyzing the angular dependence of $\boldsymbol{M}_0$ on φ_H. However, in an AFM/FM bilayer with strong interfacial exchange bias, the static magnetization $\boldsymbol{M}_0$ is noncollinear to the external magnetic field $\boldsymbol{H}_{\mathrm{ext}}$ due to the magnetic moment drag effect, i.e., $\varphi_M \neq \varphi_H$. In order to accurately obtain the SOT efficiency of AFM/FM bilayer, the key point is to analyze the angular dependence of magnetization $\boldsymbol{M}_0$ on external magnetic field $\boldsymbol{H}_{\mathrm{ext}}$.

In this work, we closely study the SOT efficiencies of IrMn/NiFe bilayers by using ST-FMR method. Firstly, we prepared a series of samples with different exchange bias field, which influences the angular dependence of ST-FMR results on $\boldsymbol{H}_{\mathrm{ext}}$, and makes the fitted curves deviate from its goal.

†Corresponding author. E-mail: weijw@lzu.edu.cn

© 2024 Chinese Physical Society and IOP Publishing Ltd

Secondly, we performed a full analysis on the IrMn/NiFe bilayer with strong exchange bias, and the angular dependence of magnetization M_0 on φ_H is determined through the minimum rule of free energy. The ST-FMR results can be thus effectively fitted. Lastly, we obtained the relative accurate SOT efficiencies of IrMn films. This work provides a useful method to analyze the SOT efficiency of AFM/FM bilayer with interfacial exchange bias field.

The sample structure is Si/SiO$_x$//NiFe (t)/IrMn (8 nm)/MgO (2 nm)/Ta (2 nm), with t = 4, 5, 6, 7, 8, 9 nm, where "//" means Si/SiO$_x$ substrate. All samples were prepared by using a magnetron sputtering system with a 1×10^{-5}-Pa base pressure. A subsequent annealing was performed at the temperature of 200 °C for 30 min in a vacuum furnace, and a static magnetic field of 5000 Oe (1 Oe = 79.5775 A·m^{-1}) was applied to the in-plane direction of samples to induce strong exchange bias and in-plane anisotropy field. The samples were then patterned into rectangular strips (100 μm×20 μm) by the standard photolithography technique and Ar ion etching. The Cr (5 nm)/Au (80 nm) electrodes were deposited to constitute the ST-FMR devices. The hysteresis loops were measured by using vibrating sample magnetometer (VSM, Lake Shore 8604). All measurements were performed at room temperature.

Figure 1(a) shows the in-plane hysteresis loops of NiFe (4 nm)/IrMn (8 nm) bilayer, which shows the sample has a remarkable exchange bias field $H_{EB}\approx135$ Oe. In the direction of hard axis, the saturation field H_s is about 500 Oe. With the increase of NiFe thickness, the exchange bias field decreases from 135 Oe to 78 Oe, as shown in Fig. 1(b), which is consistent with the previous work.[32,33]

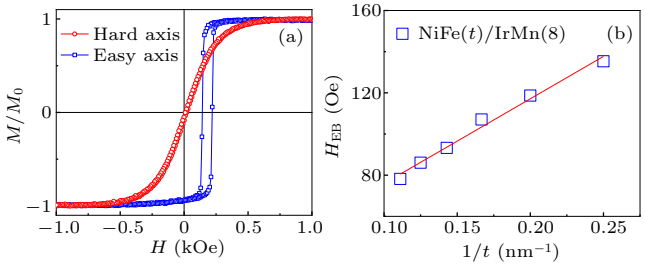


Fig. 1. (a) Normalized hysteresis loops of the sample NiFe (4 nm)/IrMn (8 nm) bilayer, in which the direction of the applied magnetic field during the annealing process is the same as the direction of the negative magnetic field during the hysteresis loop measurements. (b) The thickness dependence of exchange bias field of the samples.

Figure 2(a) shows the schematic diagram of ST-FMR setup. A radio-frequency (RF) current is injected into a sample device by ground-signal-ground (GSG) electrodes, and the current-induced SOT acts on the magnetization precession, which results in an oscillated magnetoresistance. A dc voltage signal (V_{mix}) is thus rectified through the mixing of oscillated magnetoresistance and RF current, which is fed back to the lock-in amplifier through a bias tee. A low-frequency signal is used to modulate the amplitude of RF signal and also act as a reference signal input to lock-in amplifier. The mixing voltage is measured by lock-in amplifier. The direction of exchange bias field H_{EB} and RF current J_c are parallel to the x axis. The azimuth angle between external magnetic field H_{ext} and x axis is defined as φ_H. Typical ST-FMR spectra are shown in Fig. 2(b) for the NiFe (4 nm)/IrMn (8 nm) sample with $\varphi_H=40°$, and they can be described by the equation $V_{mix}=V_s\cdot F_s+V_a\cdot F_a$, which consists of the symmetric Lorentz component $F_s(H_{ext})=\Delta H^2/[(H_{ext}-H_r)^2+\Delta H^2]$ and antisymmetric Lorentz components $F_a(H_{ext})=\Delta H(H_{ext}-H_r)/[(H_{ext}-H_r)^2+\Delta H^2]$. Here, ΔH is the resonance linewidth and H_r is the resonance field. V_s and V_a are the coefficient of the symmetric and antisymmetric components, respectively. Figure 2(c) shows the dependence of H_r on microwave frequency with the $\varphi_H=40°$ and 220°. As the microwave frequency increases, the H_r gradually moves to the higher field, which can be well fitted by Kittel equation and the effective magnetization is thus obtained (see below for details). When the microwave frequency is 6 GHz, the H_r is approximately equal to 500 Oe, which approaches to the saturation field H_s. In order to utilize the uniform precession mode based on the Stoner–Wohlfarth theory, the H_r should be larger than H_s. Therefore, we focus on the frequency above 6 GHz hereinafter. In addition, the H_r at positive field is lower than that at negative field with the same frequency, namely, the H_r at $\varphi_H=40°$ is less than that at $\varphi_H=220°$. This indicates that the resonance field is affected by the exchange bias field H_{EB}. To better understand the influence of H_{EB}, rotational measurements are performed by sweeping in-plane magnetic field along with different directions (φ_H), which also can exclude possible parasitic effects. Figures 2(d) and 2(e) show the angular dependence of H_r on φ_H at the microwave frequency $f_0=7$ GHz and 9 GHz, respectively. One can see that the resonance fields reach a maximum at the $\varphi_H=180°$, and they are approximately coincident with the angular dependence of $\cos\varphi_H$. The detailed fitting equation will be discussed in the following.

In general, the coefficients of the symmetric and antisymmetric terms can be expressed as[34–36]

$$V_s\propto\frac{\hbar\xi_{DL}J_c}{2e\mu_0M_0t_{FM}}\cos\varphi_M\sin2\varphi_M, \tag{1a}$$

$$V_a\propto\sqrt{1+\frac{4\pi M_{eff}}{H_{r0}}}\left(\frac{t_{AFM}J_c}{2}+\frac{\hbar\xi_{FL}J_c}{2e\mu_0M_0t_{FM}}\right)\times\cos\varphi_M\sin2\varphi_M, \tag{1b}$$

where $\hbar$ is the reduced Planck constant, e is the electron charge, μ_0M_0 is the saturation magnetization of Py layer, t_{FM} and t_{AFM} are the thicknesses of Py and IrMn films, respectively. $4\pi M_{eff}$ is the effective magnetization of Py layer, and H_{r0} is the effective magnetic field along the magnetization. $\xi_{DL(FL)}$ denotes the damping-like (field-like) torque efficiency. φ_M is the angle between magnetization and x axis. This angular dependence of $V_{s(a)}$ can exclude the contribution from the

spin Seebeck effect ($V_s \propto \sin\varphi_M$) and the possible unconventional spin current. By fitting the angular dependence of V_s and V_a, the average amplitude V_s^0 and V_a^0 can be obtained. Hence, the SOT efficiency ξ_{SOT} can be expressed as[28]

$$\xi_{SOT} = \frac{V_s^0}{V_a^0}\frac{e\mu_0 M_0 t_{FM} t_{AFM}}{\hbar}\sqrt{1+\frac{4\pi M_{eff}}{H_{r0}}}. \quad (2)$$

Note that the $\xi_{SOT} \approx \xi_{DL}$ when the field-like torque is much smaller than the torque of Oersted field. On the other hand, if the field-like torque is comparable to the torque of Oersted field, one can extract the ξ_{DL} and ξ_{FL} through the thickness dependence of ξ_{SOT} on t_{FM}, which is expressed as[37]

$$\frac{1}{\xi_{SOT}} = \frac{1}{\xi_{DL}}\left(1+\frac{\hbar\xi_{FL}}{e\mu_0 M_0 t_{AFM} t_{FM}}\right). \quad (3)$$

Figures 3(a) and 3(c) show the angular dependence of V_s and V_a on φ_H at $f_0 = 7$ GHz and 9 GHz, which are fitted by the above equations (1a) and (1b), respectively. Obviously, the fitted curves cannot exactly match the data points, which will affect the accuracy of measured SOT efficiency. This is because the φ_M is not equal to the φ_H due to the magnetic moment drag effect in this work. In a ferromagnetic film with in-plane magnetic isotropy, the static magnetization is collinear to the external magnetic field, i.e., $\varphi_M = \varphi_H$. In this case, equations (1a) and (1b) can be used to effectively fit the angular dependence of $V_{s(a)}$ on φ_H. However, for the case of AFM/FM bilayer with strong interfacial exchange bias, the static magnetization M_0 under the FMR condition is noncollinear to the external magnetic field, i.e., $\varphi_M \neq \varphi_H$. Hence, the φ_M as a function of φ_H needs to be obtained to accurately get the SOT efficiency of IrMn film.

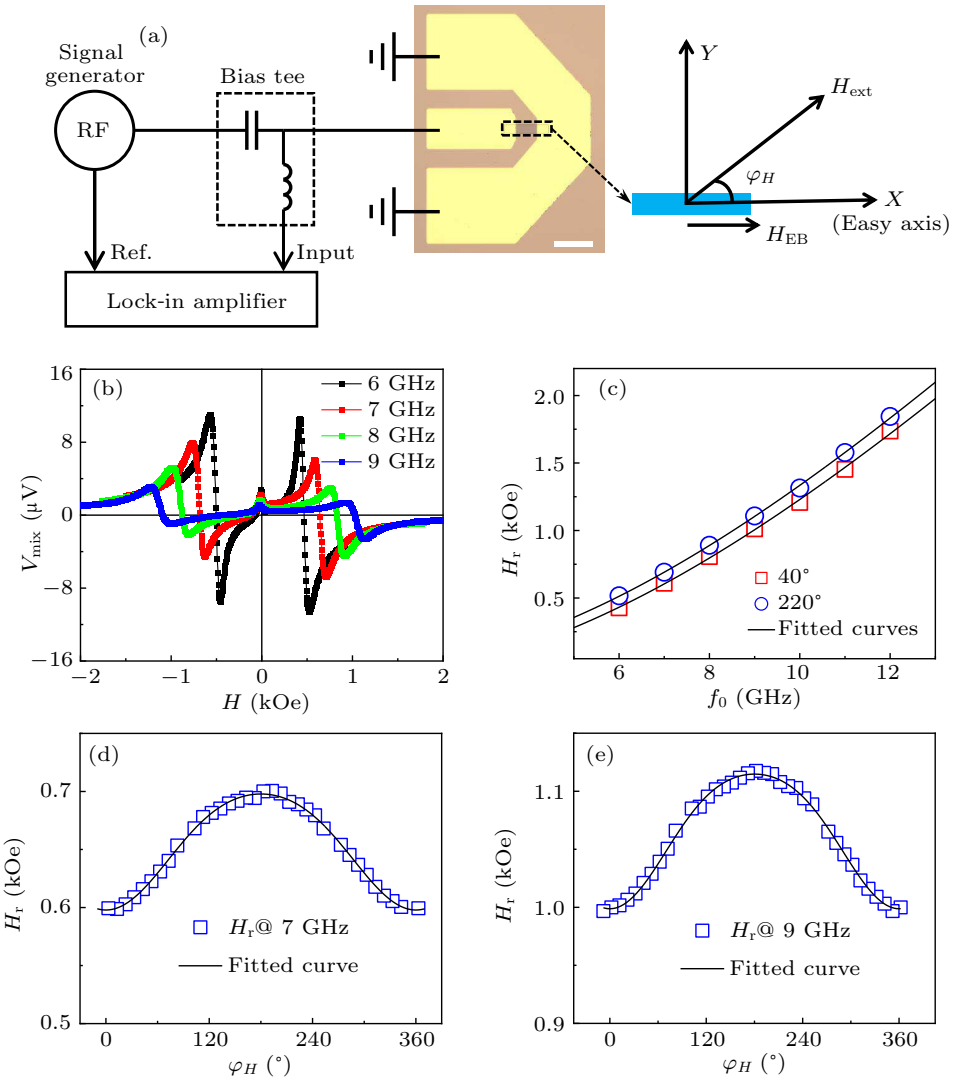


Fig. 2. (a) Schematic diagram of ST-FMR setup. The photograph shows the structure of device, and the black dotted rectangle indicates the sample under test. The length of white scale bar is 50 μm. A *xyz* coordinate system is located on the IrMn/NiFe bilayer, in which the *xy* axes are parallel to the film plane and the microwave current and exchange bias field are fixed to *x* axis. The easy axis is also parallel to the *x* axis. (b) ST-FMR spectra measured from −2 kOe to +2 kOe. (c) The frequency dependence of resonance field H_r for the NiFe (4 nm)/IrMn (8 nm) sample and the azimuth angle φ_H of external magnetic field are 40° and 220°, respectively. The black solid curves are the fitted results by Kittel equation. (d)–(e) The angular dependence of resonance field H_r on φ_H measured at $f_0 = 7$ GHz and 9 GHz, respectively, which are fitted by Eq. (8) as shown by the black solid curves.

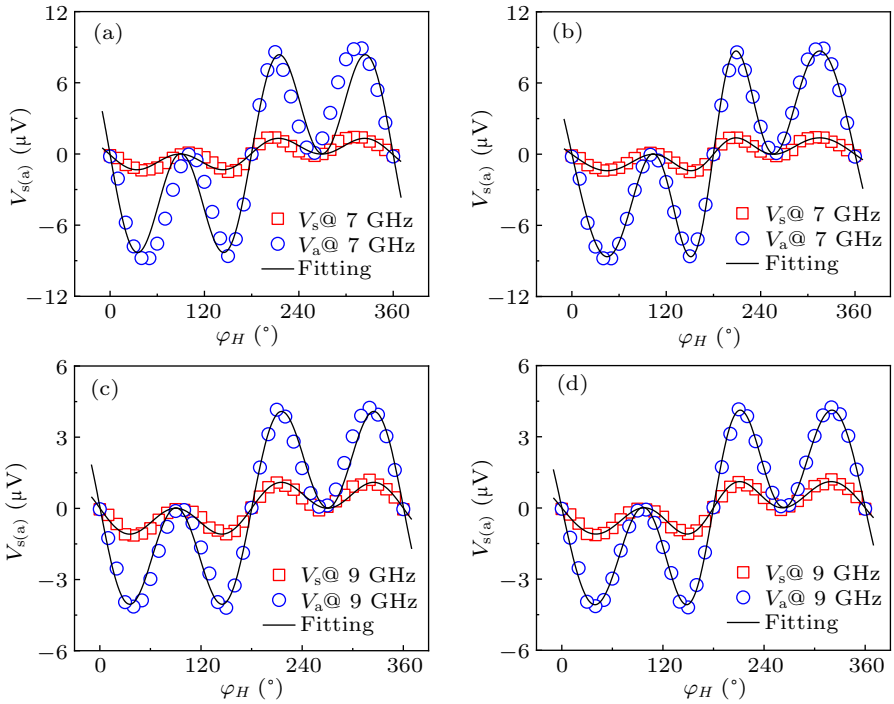


Fig. 3. The angular dependence of symmetric term V_s and antisymmetric term V_a measured at $f_0 = 7$ GHz and 9 GHz, respectively. All data are fitted by using Eq. (1): $V_{s(a)} = V^0_{s(a)} \cos\varphi_M \sin 2\varphi_M$, in which panels (a) and (c) correspond to the case of $\varphi_M = \varphi_H$, while panels (b) and (d) correspond to the case of $\varphi_M = \varphi_H + \delta$ that is given by Eq. (9).

Now, we turn to the physical model to interpret the experimental results. In order to fit the angular dependence of H_r and $V_{s(a)}$ for an FM/AFM bilayer with exchange bias field, a full analysis on this system needs to be performed. Figure 2(a) shows an *xyz* coordinate system, in which the IrMn/NiFe bilayer lies on the *xy* plane and the microwave current $\boldsymbol{J}_c$ and exchange bias field $\boldsymbol{H}_{EB}$ are parallel to *x* axis. In this regime the total free energy per unit area can be given by[38,39]

$$\begin{aligned} E \;=\; & -\mu_0 M_0 t_{FM} H_{ext} \cos(\varphi_H - \varphi_M) + K_u t_{FM} \sin^2\varphi_M \\ & + E_{AFM/FM} + E_{RA}, \end{aligned} \tag{4}$$

where K_u is the anisotropy energy of the FM layer. The first and second terms represent the Zeeman energy and anisotropy energy in the FM layer, respectively. The third term is the exchange coupling energy at the AFM/FM interface, which is written as $E_{AFM/FM} = -\mu_0 M_0 t_{FM} (H_{EB} + H_w) \cos\varphi_M$. Here the H_{EB} and H_w are the interfacial exchange bias field and the effective field of the domain-wall at the AFM side of the interface, respectively.[38] The fourth term is the contribution of the unstable antiferromagnetic grains through the rotatable anisotropy, which is written as $E_{RA} = -\mu_0 M_0 t_{FM} H_{ra} \cos^2(\varphi_H - \varphi_M)$.[38] Here H_{ra} is the effective rotatable anisotropy field in AFM.

Taking into consideration of the free energy as a function of φ_M, the minimum of free energy satisfies two conditions: $\partial E/\partial\varphi_M = 0$ and $\partial^2 E/\partial\varphi_M^2 > 0$. Accordingly, we consider the first condition, which is deduced and simplified into

$$\begin{aligned} & H_{ext} \sin(\varphi_H - \varphi_M) - \frac{H_k}{2} \sin 2\varphi_M - (H_{EB} + H_w) \sin\varphi_M \\ & + H_{RA} \sin 2(\varphi_H - \varphi_M) = 0, \end{aligned} \tag{5}$$

where the $H_k = 2K_u/(\mu_0 M_0)$ is the uniaxial anisotropy field. On the condition that the resonance field H_r is greater than the saturation field H_s, the static magnetization is noncollinear but close to the external magnetic field. Therefore, the φ_M can be expressed as the sum of φ_H and a term δ with small quantity, i.e., $\varphi_M = \varphi_H + \delta$. Equation (5) can be thus expanded through the Taylor series, and then it is reduced to a parabolic equation with respect to δ as follows:

$$\begin{aligned} & \left(\frac{H_k}{2} \sin 2\varphi_H\right) \delta^2 - (H_{ext} + 2H_{RA} \\ & + (H_{EB} + H_w) \cos\varphi_H + H_k \cos 2\varphi_H) \delta \\ & - \left(\frac{H_k}{2} \sin 2\varphi_H + (H_{EB} + H_w) \sin\varphi_H\right) = 0. \end{aligned} \tag{6}$$

By solving this parabolic equation, one can get the δ and the relation between φ_M and φ_H is thus obtained. We now discuss several situations: (i) When the azimuth angle φ_H of external magnetic field is 0 or π, the δ is equal to zero. When the φ_H is $\pi/2$ or $3\pi/2$, the δ is correspondingly equal to $\pm(H_{EB} + H_w)/[H_k - (H_{ext} + 2H_{RA})]$, respectively. This indicates that the magnetization M_0 prefers to tilt to the exchange bias field when the anisotropy field is smaller than resonance field. (ii) When the anisotropy field H_k is approximately equal to zero, the δ can be deduced to $\delta = -(H_{EB} + H_w) \sin\varphi_H / [H_{ext} + 2H_{RA} + (H_{EB} + H_w) \cos\varphi_H]$. (iii) When the $(H_k/2) \sin 2\varphi_H \neq 0$, we have two solutions through the formula of roots of a quadratic equation. Based on the above discussion, we demonstrate the angular dependence

of resonance field H_r and the symmetric (antisymmetric) term $V_{s(a)}$ in the following.

According to the Kittel's equation:

$$\left(\frac{2\pi f_0}{\gamma}\right)^2 = H_{r0}\left(H_{r0}+4\pi M_{eff}\right),$$

the H_{r0} can be derived to $H_{r0}=\sqrt{(2\pi f_0/\gamma)^2+(4\pi M_{eff}/2)^2}-4\pi M_{eff}/2$, here f_0 is the microwave frequency, γ is the gyromagnetic ratio. The H_{r0} is the effective magnetic field along the magnetization. Moreover, the H_{r0} can be also derived from the free energy, namely, Eq. (4), which can be expressed as $H_{r0}=H_{ext}\cos(\varphi_H-\varphi_M)+H_k\cos 2\varphi_M+(H_{EB}+H_w)\cos\varphi_M+H_{ra}\cos^2(\varphi_H-\varphi_M)$. Here the H_{ext} is equivalent to the resonance field H_r. Taking the $\varphi_M=\varphi_H+\delta$ and Taylor expansion into consideration, the H_{r0} can be thus expanded as

$$H_{r0}=H_r+(H_{EB}+H_w)\cos\varphi_H+H_k\cos 2\varphi_H+H_{ra}, \quad (7)$$

here, the first- and second-order terms of δ are ignored because it is much less than H_r. Consequently, the resonance field H_r can be obtained as

$$H_r=\sqrt{\left(\frac{2\pi f_0}{\gamma}\right)^2+\left(\frac{4\pi M_{eff}}{2}\right)^2}-\frac{4\pi M_{eff}}{2}-(H_{EB}+H_w)\cos\varphi_H-H_k\cos 2\varphi_H-H_{ra}. \quad (8)$$

This equation can be utilized to fit the angular dependence of resonance field H_r on φ_H, as shown in Figs. 2(d) and 2(e). Obviously, the $\cos\varphi_H$ term dominates the angular dependence of H_r and the $\cos 2\varphi_H$ term is almost zero. This suggests that the anisotropy field H_k is so small that it can be ignored. The $H_{EB}+H_w\approx 58$ Oe and $H_{r0}-H_{ra}\approx 1063$ Oe are then obtained from the fitted results. Note that this H_{EB} value is smaller than that obtained from hysteresis loop, which is like caused by the nonuniform resonance field shift[40] and the fabrication process of device.[41,42] By performing the rotational measurements at different microwave frequency f_0, we can get the $4\pi M_{eff}$ by employing the Kittel's equation to fit the relation between the obtained H_{r0} and f_0. The $4\pi M_{eff}$ and H_{r0} are useful for calculating the SOT efficiency through Eq. (2). Due to the neglect of H_k, the δ can be determined by

$$\delta=\frac{-(H_{EB}+H_w)\sin\varphi_H}{H_r+2H_{RA}+(H_{EB}+H_w)\cos\varphi_H},$$

and the φ_M is thus expressed as

$$\varphi_M=\varphi_H-\frac{(H_{EB}+H_w)\sin\varphi_H}{H_{r0}+H_{RA}}. \quad (9)$$

Substituting this expression into Eqs. (1a) and (1b), they can be utilized to fit the angular dependence of $V_{s(a)}$ on φ_H, as shown in Figs. 3(b) and 3(d). The fitted curves match well with the data points, which demonstrates that the above physical model and equation (9) are suitable for the AFM/FM system with strong exchange bias. The average amplitude V_s^0 and V_a^0 are then obtained, which are taken into Eq. (2) to deduce the SOT efficiencies of samples. From the fitting parameters for the 7 GHz, the V_s^0/V_a^0 is equal to 0.158 and 0.160, respectively. We can thus obtain the difference of SOT efficiencies after the correction is about 1.3%.

Figure 4(a) shows the SOT efficiencies of the NiFe (4 nm)/IrMn (8 nm) bilayer at different microwave frequencies. As the frequency increases from 7 GHz to 12 GHz, the SOT efficiency ξ_{SOT} gradually increases and then saturates above 9 GHz. The saturated ξ_{SOT} is about 0.07. In order to extract the damping-like torque efficiency ξ_{DL} and field-like torque efficiency ξ_{FL}, a linear fit between $1/\xi_{SOT}$ and $1/t_{FM}$ is performed by using Eq. (3), as shown in Fig. 4(b). The fitted results show that the $\xi_{DL}=0.058\pm0.010$ and $\xi_{FL}=-0.005\pm0.011$ for the IrMn/NiFe bilayers. The ξ_{FL} has a value less than its error value, which suggests that the field-like torque is so small that it can be ignored in the IrMn/NiFe samples, and the SOT is mainly attributed to the damping-like torque from the bulk of IrMn films. This ξ_{DL} value is consistent with the previous works ($\xi_{DL}=0.028$–0.083 for the polycrystalline IrMn).[10,12,24]

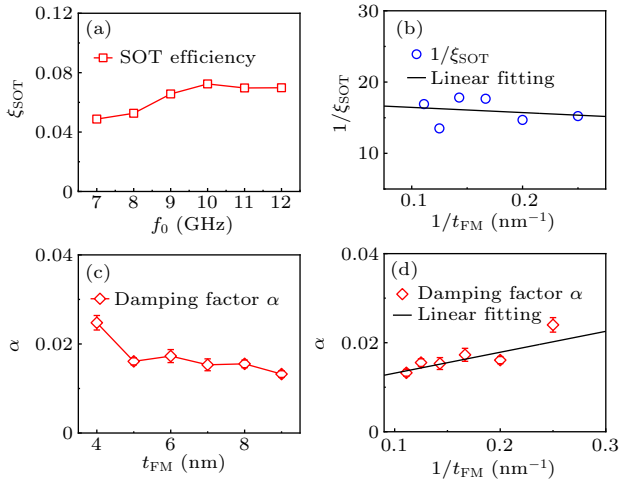


Fig. 4. (a) The frequency dependence of SOT efficiency for the NiFe(5 nm)/IrMn(8 nm) sample. (b) The relationship between the reciprocal of SOT efficiency and the reciprocal of the thickness of ferromagnetic layer. The black solid line denotes the linear fitting result. (c) The damping factor α as a function of the thickness of ferromagnetic layer. (d) The relationship between the damping factor and the reciprocal of the thickness of ferromagnetic layer, which can be fitted by a linear equation, as shown by the black solid line.

To further obtain the spin Hall angle θ_{SH} of IrMn film, the interfacial spin transparency T_{in} needs to be estimated. The correlation between ξ_{DL} and T_{in} is $\xi_{DL}=T_{in}\theta_{SH}$. Normally, the T_{in} is less than unity because of the finite spin mixing conductance at the interface, which can be determined by[43–45]

$$T_{in}=\frac{2G^{\uparrow\downarrow}\tanh(t_{AFM}/2\lambda_{sd})}{G+2G^{\uparrow\downarrow}\coth(t_{AFM}/\lambda_{sd})}.$$

Here $G^{\uparrow\downarrow}$ is the interfacial spin mixing conductance and $G \equiv \sigma/\lambda_{sd}$ is the spin conductance of IrMn film, where σ and λ_{sd} are the electrical conductivity and spin diffusion length of IrMn film, respectively. The $G^{\uparrow\downarrow}$ can be estimated from the Gilbert damping α of IrMn/NiFe bilayers with various NiFe thicknesses. Figure 4(c) shows the thickness dependence of damping factor. With the increase of the thickness of NiFe layer, the damping factor decreases gradually. The dependence of damping α on $1/t_{FM}$ exhibits a linear relation, as shown in Fig. 4(d), which can be fitted by $\alpha = \alpha_0 + (G_{eff}^{\uparrow\downarrow}\gamma\hbar^2/2e^2M_0)t_{FM}^{-1}$.[46,47] Here $G_{eff}^{\uparrow\downarrow}$ is the effective spin mixing conductance, which can be expressed as $G_{eff}^{\uparrow\downarrow} = G^{\uparrow\downarrow}/(1+2G^{\uparrow\downarrow}/G)$. We then obtain the intrinsic damping $\alpha_0 = 8.4\times10^{-3}$ and effective spin mixing conductance $G_{eff}^{\uparrow\downarrow} = 8.5\times10^{15}\ \Omega^{-1}\cdot m^{-2}$ for the IrMn/NiFe bilayers. Utilizing the $\lambda_{sd} = 0.7$ nm in Ref. [23] and $\sigma = 1.6\times10^{6}\ \Omega^{-1}\cdot m^{-1}$ measured by four-terminal method, the interfacial spin transparency T_{in} can be obtained to be 0.87 and the spin Hall angle θ_{SH} of IrMn film is thus determined to be 0.067. This work provides a useful method to analyze the angular dependence of ST-FMR results and facilitates the accurate measurement of SOT efficiency for the AFM/FM heterostructures with strong exchange bias.

In summary, we have performed a full analysis on the AFM/FM systems with strong interfacial exchange bias, and the angular relationship between φ_H and φ_M has been obtained through the minimum rule of free energy. Based on this model, we have studied the SOT efficiencies of IrMn/NiFe bilayers by using ST-FMR method, and the results can be well fitted. Finally, the relative accurate SOT efficiency $\xi_{DL} = 0.058$ and interfacial spin transparency $T_{in} = 0.87$ for the IrMn/NiFe bilayers have been obtained. This work provides a useful method to analyze the angular dependence of ST-FMR results on the condition of magnetic moment drag effect, which is not only applicable for the AFM/FM heterostructures with strong exchange bias, but also suitable for the FM film with strong magnetocrystalline anisotropy.

Acknowledgements

Project supported by the National Key Research and Development Program of China (Grant No. 2021YFB3601300), the National Natural Science Foundation of China (Grant Nos. 52201290, 12074158, and 12174166), and the Fundamental Research Funds for the Central Universities (Grant No. lzujbky-2022-kb01).

References

[1] Baltz V, Manchon A, Tsoi M, Moriyama T, Ono T and Tserkovnyak Y 2018 *Rev. Mod. Phys.* **90** 015005
[2] Manchon A, Železný J, Miron I M, Jungwirth T, Sinova J, Thiaville A, Garello K and Gambardella P 2019 *Rev. Mod. Phys.* **91** 035004
[3] Železný J, Wadley P, Olejník K, Hoffmann A and Ohno H 2018 *Nat. Phys.* **14** 220
[4] Qiu H, Zhou L, Zhang C, Wu J, Tian Y, Cheng S, Mi S, Zhao H, Zhang Q, Wu D, Jin B, Chen J and Wu P 2021 *Nat. Phys.* **17** 388
[5] Vaidya P, Morley S A, Tol J van, Liu Y, Cheng R, Brataas A, Lederman D and Barco E del 2020 *Science* **368** 160
[6] Mendes J B S, Cunha R O, Santos O A, Ribeiro P R T, Machado F L A, Rodríguez-Suárez R L, Azevedo A and Rezende S M 2014 *Phys. Rev. B* **89** 140406
[7] Ou Y, Shi S, Ralph D C and Buhrman R A 2016 *Phys. Rev. B* **93** 220405
[8] Arana M, Gamino M, Silva E F, Barthem V M T S, Givord D, Azevedo A and Rezende S M 2018 *Phys. Rev. B* **98** 144431
[9] Chen X, Shi S, Shi G, Fan X, Song C, Zhou X, Bai H, Liao L, Zhou Y, Zhang H, Li A, Chen Y, Han X, Jiang S, Zhu Z, Wu H, Wang X, Xue D, Yang H and Pan F 2021 *Nat. Mater.* **20** 800
[10] Saglam H, Rojas-Sanchez J C, Petit S, Hehn M, Zhang W, Pearson J E, Mangin S and Hoffmann A 2018 *Phys. Rev. B* **98** 094407
[11] Yang Y, Xu Y, Zhang X, Wang Y, Zhang S, Li R W, Mirshekarloo M S, Yao K and Wu Y 2016 *Phys. Rev. B* **93** 094402
[12] Zhou J, Wang X, Liu Y, Yu J, Fu H, Liu L, Chen S, Deng J, Lin W, Shu X, Yoong H Y, Hong T, Matsuda M, Yang P, Adams S, Yan B, Han X and Chen J 2019 *Sci. Adv.* **5** eaau6696
[13] Zhou J, Shu X Y, Liu Y H, Wang X, Lin W N, Chen S H, Liu L, Xie Q D, Hong T, Yang P, Yan B H, Han X F and Chen J S 2020 *Phys. Rev. B* **101** 184403
[14] Bai H, Zhou X F, Zhang H W, Kong W W, Liao L Y, Feng X Y, Chen X Z, You Y F, Zhou Y J, Han L, Zhu W X, Pan F, Fan X L and Song C 2021 *Phys. Rev. B* **104** 104401
[15] Nan T, Quintela C X, Irwin J, Gurung G, Shao D F, Gibbons J, Campbell N, Song K, Choi S Y, Guo L, Johnson R D, Manuel P, Chopdekar R V, Hallsteinsen I, Tybell T, Ryan P J, Kim J W, Choi Y, Radaelli P G, Ralph D C, Tsymbal E Y, Rzchowski M S and Eom C B 2020 *Nat. Commun.* **11** 4671
[16] Hazra B K, Pal B, Jeon J C, Neumann R R, Gobel B, Deniz H, Styervoyedov A, Meyerheim H, Mertig I, Yang S H and Parkin S S P 2023 *Nat. Commun.* **14** 4549
[17] Liang S, Han L, You Y, Bai H, Pan F and Song C 2023 *Phys. Rev. B* **107** 184427
[18] You Y, Bai H, Feng X, Fan X, Han L, Zhou X, Zhou Y, Zhang R, Chen T, Pan F and Song C 2021 *Nat. Commun.* **12** 6524
[19] van den Brink A, Vermijs G, Solignac A, Koo J, Kohlhepp J T, Swagten H J M and Koopmans B 2016 *Nat. Commun.* **7** 10854
[20] Fukami S, Zhang C, DuttaGupta S, Kurenkov A and Ohno H 2016 *Nat. Mater.* **15** 535
[21] Razavi S A, Wu D, Yu G, Lau Y C, Wong K L, Zhu W, He C, Zhang Z, Coey J M D, Stamenov P, Amiri P K and Wang Kang L 2017 *Phys. Rev. Appl.* **7** 024023
[22] Grochot K, Karwacki Ł, Łazarski S, Skowroński W, Kanak J, Powroźnik W, Kuświk P, Kowacz M, Stobiecki F and Stobiecki T 2021 *Phys. Rev. Appl.* **15** 014017
[23] Tshitoyan V, Ciccarelli C, Mihai A P, Ali M, Irvine A C, Moore T A, Jungwirth T and Ferguson A J 2015 *Phys. Rev. B* **92** 214406
[24] Zhang W, Jungfleisch M B, Freimuth F, Jiang W, Sklenar J, Pearson J E, Ketterson J B, Mokrousov Y and Hoffmann A 2015 *Phys. Rev. B* **92** 144405
[25] Zhang W, Jungfleisch M B, Jiang W, Pearson J E, Hoffmann A, Freimuth F and Mokrousov Y 2014 *Phys. Rev. Lett.* **113** 196602
[26] Liu L, Moriyama T, Ralph D C and Buhrman R A 2011 *Phys. Rev. Lett.* **106** 036601
[27] Mellnik A R, Lee J S, Richardella A, Grab J L, Mintun P J, Fischer M H, Vaezi A, Manchon A, Kim E A, Samarth N and Ralph D C 2014 *Nature* **511** 449
[28] Wei J, He C, Wang X, Xu H, Liu Y, Guang Y, Wan C, Feng J, Yu G and Han X 2020 *Phys. Rev. Appl.* **13** 034041
[29] Avci C O, Garello K, Gabureac M, Ghosh A, Fuhrer A, Alvarado S F and Gambardella P 2014 *Phys. Rev. B* **90** 224427
[30] Hayashi M, Kim J, Yamanouchi M and Ohno H 2014 *Phys. Rev. B* **89** 144425
[31] Wang X, Tang J, Xia X, He C, Zhang J, Liu Y, Wan C, Fang C, Guo C, Yang W, Guang Y, Zhang X, Xu H, Wei J, Liao M, Lu X, Feng J, Li X, Peng Y, Wei H, Yang R, Shi D, Zhang X, Han Z, Zhang Z, Zhang G, Yu G and Han X 2019 *Sci. Adv.* **5** eaaw8904
[32] Jungblut R, Coehoorn R, Johnson M T, aan de Stegge J and Reinders A 1994 *J. Appl. Phys.* **75** 6659
[33] Shi Z, Du J and Zhou S M 2014 *Chin. Phys. B* **23** 027503
[34] MacNeill D, Stiehl G M, Guimaraes M H D, Buhrman R A, Park J and Ralph D C 2017 *Nat. Phys.* **13** 300

[35] Okada A, Takeuchi Y, Furuya K, Zhang C, Sato H, Fukami S and Ohno H 2019 *Phys. Rev. Appl.* **12** 014040
[36] Xu H, Wei J, Zhou H, Feng J, Xu T, Du H, He C, Huang Y, Zhang J, Liu Y, Wu H C, Guo C, Wang X, Guang Y, Wei H, Peng Y, Jiang W, Yu G and Han X 2020 *Adv. Mater.* **32** 2000513
[37] Ou Y, Pai C F, Shi S, Ralph D C and Buhrman R A 2016 *Phys. Rev. B* **94** 140414
[38] Arana M, Gamino M, Oliveira A B, Holanda J, Azevedo A, Rezende S M and Rodríguez-Suárez R L 2020 *Phys. Rev. B* **102** 104405
[39] Xi H, Mountfield K R and White R M 2000 *J. Appl. Phys.* **87** 4367
[40] Stiles M D and McMichael R D 1999 *Phys. Rev. B* **59** 3722
[41] Shen Y, Wu Y, Xie H, Li K, Qiu J and Guo Z 2002 *J. Appl. Phys.* **91** 8001
[42] Liu F and Ross C A 2014 *J. Appl. Phys.* **116** 194307
[43] Shao Q, Tang C, Yu G, Navabi A, Wu H, He C, Li J, Upadhyaya P, Zhang P, Razavi S A, He Q, Liu Y, Yang P, Kim S K, Zheng C, Liu Y, Pan L, Lake R K, Han X, Tserkovnyak Y, Shi J and Wang Kang L 2018 *Nat. Commun.* **9** 3612
[44] Zhu L, Ralph D C and Buhrman R A 2019 *Phys. Rev. Lett.* **123** 057203
[45] Wei J, Zhong H, Liu J, Wang X, Meng F, Xu H, Liu Y, Luo X, Zhang Q, Guang Y, Feng J, Zhang J, Yang L, Ge C, Gu L, Jin K, Yu G and Han X 2021 *Adv. Funct. Mater.* **31** 2100380
[46] Heinrich B, Burrowes C, Montoya E, Kardasz B, Girt E, Song Y Y, Sun Y and Wu M 2011 *Phys. Rev. Lett.* **107** 066604
[47] Berger A J, Edwards E R J, Nembach H T, Karis O, Weiler M and Silva T J 2018 *Phys. Rev. B* **98** 024402